

UNCLASSIFIED

AD 428563

DEFENSE DOCUMENTATION CENTER

FOR

SCIENTIFIC AND TECHNICAL INFORMATION

CAMERON STATION, ALEXANDRIA, VIRGINIA



UNCLASSIFIED

NOTICE: When government or other drawings, specifications or other data are used for any purpose other than in connection with a definitely related government procurement operation, the U. S. Government thereby incurs no responsibility, nor any obligation whatsoever; and the fact that the Government may have formulated, furnished, or in any way supplied the said drawings, specifications, or other data is not to be regarded by implication or otherwise as in any manner licensing the holder or any other person or corporation, or conveying any rights or permission to manufacture, use or sell any patented invention that may in any way be related thereto.

AEDC-TDR-64-29

428563

CATALOGED BY DDC

428563

428563



**A GENERAL METHOD FOR NUMERICAL INTEGRATION
THROUGH A SADDLE-POINT SINGULARITY
WITH APPLICATION TO ONE-DIMENSIONAL
NONEQUILIBRIUM NOZZLE FLOW**

By

George Emanuel

Department of Aeronautics and Astronautics
Stanford University
Stanford, California

TECHNICAL DOCUMENTARY REPORT NO. AEDC-TDR-64-29

January 1964

Program Element 62405334/8952, Task 895210

(Prepared under Contract No. AF 40(600)-930 by Stanford University,
Stanford, California.)

ARNOLD ENGINEERING DEVELOPMENT CENTER

DDC

AIR FORCE SYSTEMS COMMAND

UNITED STATES AIR FORCE

FEB 4 1964

TISIA B

NOTICES

Qualified requesters may obtain copies of this report from DDC, Cameron Station, Alexandria, Va. Orders will be expedited if placed through the librarian or other staff member designated to request and receive documents from DDC.

When Government drawings, specifications or other data are used for any purpose other than in connection with a definitely related Government procurement operation, the United States Government thereby incurs no responsibility nor any obligation whatsoever; and the fact that the Government may have formulated, furnished, or in any way supplied the said drawings, specifications, or other data, is not to be regarded by implication or otherwise as in any manner licensing the holder or any other person or corporation, or conveying any rights or permission to manufacture, use, or sell any patented invention that may in any way be related thereto.

A GENERAL METHOD FOR NUMERICAL INTEGRATION
THROUGH A SADDLE-POINT SINGULARITY
WITH APPLICATION TO ONE-DIMENSIONAL
NONEQUILIBRIUM NOZZLE FLOW

By

George Emanuel

Department of Aeronautics and Astronautics

Stanford University

Stanford, California

(The reproducibles used in the reproduction of this report
were supplied by the author.)

January 1964

ABSTRACT

The work described is a continuation of that reported previously in AEDC-TN-61-65, AEDC-TDR-62-131, and AEDC-TDR-63-82. The present report contains a general method for integrating numerically through a saddle-point singularity of an ordinary differential equation. The solution of the differential equation is assumed to depend also on the value of a parameter, such as the mass flow. The method is thus applicable to a wide assortment of gas-dynamic problems including one-dimensional nonequilibrium nozzle flow and two-phase nozzle flow.

Specific application is made to nonequilibrium nozzle flow, and the results of this application are presented and discussed. The method proved to be numerically accurate without requiring an exceedingly precise estimate for the critical mass flow.

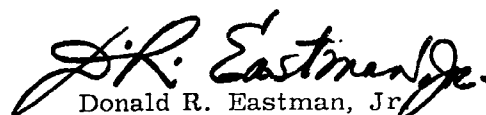
The work also includes a modification of the method for calculating approximate equilibrium nozzle flows first given in AEDC-TDR-62-131.

PUBLICATION REVIEW

This report has been reviewed and publication is approved.



Jay T. Edwards, III
Capt, USAF
Gas Dynamics Division
DCS/Research



Donald R. Eastman, Jr.
DCS/Research

CONTENTS

	<u>Page</u>
ABSTRACT	iii
SYMBOLS	vi
1.0 INTRODUCTION	1
2.0 OPTIMUM-POINT METHOD	4
3.0 APPLICATION TO NONEQUILIBRIUM NOZZLE FLOW	7
4.0 RESULTS AND DISCUSSION	20
REFERENCES	26
APPENDIXES	
I ANALYTICAL EXPRESSIONS FOR $A_{IV}(x)$	27
II MODIFICATION OF THE APPROXIMATE EQUILIBRIUM METHOD OF PART II	29
FIGURES	31

SYMBOLS

PRIMARY SYMBOLS

A	nozzle area
A_g	given nozzle area
c_o	defined by equation (3-37)
c_{p_i}	specific heat of translation and rotation at constant pressure per mole of species i
E	percent error defined by equation (3-9)
e_{D_i}	energy of reaction per mole of species i
e_{v_i}	vibrational energy per mole of species i
f_i	defined in Section 3.5
h	integration step size
h	enthalpy per unit mass of fluid
h_t	stagnation enthalpy per unit mass of fluid
M_f	Mach number based on the frozen speed of sound
m	mass flow per unit time
m_{eq}	mass flow per unit time for the equilibrium-flow solution
m_f	mass flow per unit time for the frozen-flow solution
N	defined by equation (1-3)
N_l	total number of chemical species
n_i	mole-mass ratio of species i ; that is, number of moles of species i per unit mass of fluid
$n_{i,eq}$	value of n_i for the equilibrium-flow solution
P, Q	defined by equation (2-1)
R	universal gas constant
T	static temperature

u	flow speed
V	length of region IV
V_i	input parameters defined in Chapter 3
X_{PQ}	parameter defined by equation (2-5)
x	distance along nozzle axis
x, y	variables in equation (2-1)
\bar{x}	defined by equation (3-18)
α	parameter defined in Chapter 2
γ	ratio of specific heats
η_i	constants defined in Section 3.5
$\lambda_1(\bar{x})$	function defined by equation (3-19)
$\lambda_2(\bar{x})$	function defined by equation (3-21)
ρ	mass density of fluid
ϕ	defined by equation (3-4)

SUPERSCRIPTS AND SUBSCRIPTS

$()^*$	value at the saddle-point singularity
$()^*$	value at an extremum of $\lambda_1(\bar{x})$
$()'$	denotes differentiation with respect to \bar{x}
$()^+$	value at the preceding integration step $x - h$
$()^{++}$	value at $x - 2h$
a, b	defined in Section 3.7
cr	value associated with the critical solution
f	frozen-flow value
i	value for species i

o	value at the initial point
opt	value at the optimum point
th	value at the nozzle throat
tr	value at the transfer point
III	value associated with region III
IV	value associated with region IV

1.0 INTRODUCTION

This is the fourth and final report in a series concerning the calculation of the reacting flow of a complex gas in the nozzle of a hypersonic wind tunnel. The preceding three reports, hereafter referred to as Parts I, II, and III, dealt with the following topics:

- (a) Part I, by Vincenti (1961), describes a five-species model for air, governed by eight chemical kinetic reactions. A method is given for the numerical calculation of the one-dimensional nonequilibrium flow of this gas through a hypersonic nozzle. A specific calculation carried out on a high-speed digital computer revealed that the method required too much computer time to be practical for engineering purposes.
- (b) Part II, by Emanuel and Vincenti (1962), describes a method for calculating equilibrium nozzle flows. The method is simple, but requires a large amount of machine time. This report also contains an approximate but relatively simple method for calculating equilibrium nozzle flows.
- (c) Part III, by Emanuel (1963), contains the analytical basis for the numerical method described in Part II. The report is thus concerned primarily with the interaction of a "stiff", ordinary differential equation and various integration procedures.

The method described in Part II requires that the forward integration of the nonequilibrium equations proceed from an initial point that is in equilibrium. This point is chosen somewhat upstream of the nozzle location at which the chemistry first departs appreciably from the equilibrium-flow solution. For a sufficiently high stagnation pressure, this point may be taken in the supersonic portion of the nozzle. In this situation the nonequilibrium flow is readily calculated by the method given in Part II. For low stagnation pressures, however, the chemistry first departs from the equilibrium-flow solution at a subsonic nozzle location, and the forward integration of the equations must now proceed from a subsonic initial point. In this case the method given in Part II must be modified to incorporate a procedure for dealing with the singularity that occurs at the sonic point. This report describes in detail one such method.

The sonic-point singularity occurs in both frozen and nonequilibrium nozzle flows. In both instances it is a saddle point that occurs when the numerator and denominator of the right-hand side of an ordinary differential equation simultaneously become zero. The differential equation involved is a gas-dynamic one. In the frozen-flow case, for example, it is given by

$$\frac{dT}{dx} = \frac{(\gamma-1)T M_F^2 \left(\frac{1}{A} \frac{dA}{dx} \right)}{1 - M_F^2}, \quad (1-1)$$

where T is the temperature, x the distance along the nozzle axis, γ the ratio of specific heats, M_F the Mach number based on the frozen speed of sound, and A the nozzle area. For frozen flow, the location of the singularity is at the throat and the critical mass flow is easily determined. Equation (1-1) assumes that the nozzle area is a given function of x , as is generally the case, while the temperature is the unknown dependent variable. If the role of the two variables is interchanged, i.e., the temperature is a given function of x and the area is the unknown dependent variable, then the singularity is removed. This result is evident when equation (1-1) is rewritten as follows:

$$\frac{dA}{dx} = \frac{(1 - M_F^2) A \left(\frac{1}{T} \frac{dT}{dx} \right)}{(\gamma-1) M_F^2} \quad (1-2)$$

Thus, the singularity in one-dimensional nozzle flow occurs only when the doubled-valued variable A is taken as the given function of x .

In nonequilibrium nozzle flow the situation is more complicated. In particular, the location of the saddle point and the critical mass flow are not known a priori. It is therefore necessary to guess a value for the mass flow before starting the numerical integration. This value, of course, will probably differ from the critical one, and the resulting solution will either be subsonic for the entire nozzle, or an infinity, which terminates the solution, will occur upstream of the singularity.

The problem dealt with in this report may be stated as follows: A solution is to be obtained that passes smoothly through the saddle-point singularity of an ordinary differential equation. This solution furthermore depends on a parameter, such as the mass flow, whose precise value is unknown. As such, this problem is encountered not only in computing nonequilibrium nozzle or diffuser flow but occurs also in two-phase nozzle or diffuser flow (see Glauz (1962)). It also appears in inviscid flow about a two-dimensional or axisymmetric blunt body in a supersonic stream when such flow is computed by the method of integral relations (see Belotserkovskii (1957) and (1958) or Xerikos and Anderson (1962)).

A general solution to the foregoing problem is outlined in Chapter 2. This solution takes the form of a well-defined numerical method, hereafter referred to as the optimum-point method, that is well suited for use with high-speed digital computers. The method has the important advantages of being relatively simple to apply, not requiring

an exceedingly precise estimate of the parameter, and yielding a numerically accurate solution. Specific application, described in Chapter 3 and in Appendix I, was made to nonequilibrium nozzle flows. Numerous calculations on an IBM 7090 computer verified the simplicity and accuracy of the method in this application. The results of one of these, along with the corresponding equilibrium nozzle-flow solution, is presented in Chapter 4. This chapter also discusses certain gas-dynamic results stemming from this calculation. Finally, Appendix II modifies the approximate equilibrium method first presented in Part II.

The singularity problem can also be attacked by means of trial-and-error procedures, wherein numerous integrations are performed, each with a slightly different value for the mass flow (see, for example, Reichenbach (1960)). Once a subsonic solution is available that is sufficiently close to the critical one, the integration can then be started from a supersonic initial point obtained by extrapolating the subsonic solution across the singularity. This approach, however, consumes a considerable amount of computer time and generally results in a more accurate estimate for the critical mass flow than is actually needed.

Other methods also exist for dealing with saddle-point singularities. These methods are applicable only in special circumstances. For example, Eschenroeder, Boyer and Hall (1962) outline a method for dealing with the singularity in nonequilibrium nozzle flow. Their method is based on the assumption that the nonequilibrium value for the density differs negligibly from its equilibrium-flow value in the subsonic portion of the nozzle. The equilibrium value of the density is then used as the independent variable to calculate the subsonic portion of the nozzle. Another special method designed for two-phase flows is due to Glauz (1962). This method introduces a new dependent variable N defined by

$$N \equiv \frac{1}{2} (M_F^2 - 1)^2. \quad (1-3)$$

Transformation (1-3) does remove the singularity from equation (1-1). The transformed equation, however, must now simultaneously satisfy the interior-boundary conditions $N = 0$ and $(dN/dx) = 0$.

The author wishes to express his sincere gratitude to Professor Walter G. Vincenti for his encouragement and assistance. Thanks are also due to Mrs. Lita Emanuel for editorial assistance and to Messrs. H. L. Mitchell and Lyle B. Smith for computer programming. During the work the author was supported in part by a research grant to Stanford University from the National Science Foundation.

2.0 OPTIMUM-POINT METHOD

Before the optimum-point method is described in its simplest form, some pertinent facts concerning saddle points will be presented. Consider the single ordinary differential equation

$$\frac{dy}{dx} = \frac{P(x,y)}{Q(x,y)} \quad (2.1)$$

with the initial condition $y(x_0) = y_0$. In addition, let the right-hand side of equation (2-1) depend on a parameter α not explicitly shown in the equation. Consequently, the solution of equation (2.1),

$$y = y(x;\alpha), \quad (2-2)$$

depends on α . We also require that for a unique value of α , referred to as the critical value α_{cr} , the differential equation has a saddle point at (x^*, y^*) , as shown in Figure 1. For values of α different from α_{cr} , the integral curves lie either above or below the critical solution $y_{cr} = y(x; \alpha_{cr})$. Only two solutions of equation (2-1) actually pass through the saddle point. One of these originates at a point above y^* , while the other originates below. We may restrict the discussion to the case $y_0 > y^*$ without loss of generality.

In general, the critical value of α is not known a priori. In this case, for some value of α , say α_1 (see Figure 1), the integral curve $y(x; \alpha_1)$ has a minimum where $P(x, y(x; \alpha_1))$ is zero. This zero generally does not occur at $x = x^*$. Similarly, each integral curve below the critical one has a point where Q is zero and the slope is infinite. This zero does not generally occur at $y = y^*$. Thus, the exact location of the saddle point (x^*, y^*) is also not known a priori.

It is well known that the critical solution in a neighborhood of the saddle point is linear. The slope of the critical solution at the saddle point can be determined if L'Hospital's rule can be applied to the indeterminate form P/Q . When the location of the saddle point is not known a priori, however, L'Hospital's rule cannot be applied directly.

Finally, we note that if α is close to α_{cr} , then the integral curve $y(x; \alpha)$ remains close to y_{cr} until either P or Q is nearly zero. Furthermore, the slope $dy(x; \alpha)/dx$ also remains close to dy_{cr}/dx until the integral curve $y(x; \alpha)$ approaches the saddle point. Thus, if α is sufficiently close to α_{cr} , there will exist a point (x_{opt}, y_{opt}) on $y = y(x; \alpha)$, close to the saddle point, where the slope $dy(x; \alpha)/dx$ best approximates the slope of the critical solution evaluated at the saddle point. The function of the optimum-point method is to locate this point. It must be re-emphasized that the location of the optimum-point cannot depend explicitly on the critical value α_{cr} , on

the location of the saddle point (x^*, y^*) , or on the slope of the critical solution at the saddle point, since all these quantities are unknown.

The actual location of the optimum point depends on a criterion based on L'Hospital's rule. When this rule is applied to equation (2-1), we obtain

$$\frac{dy}{dx} = -\frac{\frac{dP}{dx}}{\frac{dQ}{dx}}, \quad (2-3)$$

where the derivative $d(\)/dx$ is given by

$$\frac{d}{dx} = \frac{\partial}{\partial x} + \frac{dy}{dx} \frac{\partial}{\partial y}.$$

When dy/dx is eliminated from equations (2-1) and (2-3), the following result is obtained:

$$\frac{P}{\frac{dP}{dx}} - \frac{Q}{\frac{dQ}{dx}} = 0. \quad (2-4)$$

This result is exact, of course, only at the saddle point. The left-hand side of equation (2-4), which has the same dimensions as x , in general is not zero when evaluated away from the saddle point. A new parameter X_{PQ} is therefore defined as

$$X_{PQ} = \frac{P}{\frac{dP}{dx}} - \frac{Q}{\frac{dQ}{dx}}. \quad (2-5)$$

This parameter is evaluated along a specific integral curve during the forward integration of equation (2-1). How X_{PQ} is evaluated numerically is discussed in the next chapter. The optimum point is then defined as the point nearest to (x^*, y^*) where $|X_{PQ}|$ is a minimum.

We now indicate why one of the several minimum values of $|X_{PQ}|$ that may occur gives the point at which the slope $dy(x; \alpha)/dx$ best approximates the slope of the critical solution evaluated at the saddle point. We first assume that P and Q are continuously differentiable, as is generally the case. Next, let us rewrite X_{PQ} as follows:

$$X_{PQ} = \frac{Q}{\frac{dP}{dx}} \left(\frac{dy}{dx} - \frac{\frac{dP}{dx}}{\frac{dQ}{dx}} \right).$$

Since P and Q are continuously differentiable, the ratio $(dP/dx)/(dQ/dx)$ may be evaluated at the saddle point, which is assumed to be close to the optimum point. The quantity in parentheses is then approximately the difference between the slope $dy(x;\alpha)/dx$ and the slope of the critical solution at the saddle point. Therefore, this minimum value of $|X_{PQ}|$ corresponds to the optimum point.

As α tends toward α_{cr} , the integral curve $y = y(x;\alpha)$ tends toward the critical solution. Thus, the optimum point will also tend toward the saddle point as shown by the dots in Figure 1. All of the non-equilibrium nozzle-flow calculations carried out in the course of this work are in accord with the foregoing conclusions.

On the basis of the foregoing ideas, an approximate numerical solution that passes through the saddle point can be constructed as follows:

- (a) The numerical integration of equation (2-1), for a particular value of α , proceeds from (x_0, y_0) until the optimum point is reached.
- (b) For values of x in an interval $x_{opt} \leq x \leq x_{tr}$, where the transfer point x_{tr} is defined as some suitable point greater than x^* , the linear approximation

$$y = (x - x_{opt}) \left(\frac{dy}{dx} \right)_{opt} + y_{opt} \quad (2-6)$$

is used.

- (c) For values of x greater than x_{tr} equation (2-1) is again integrated numerically with the initial condition

$$y(x_{tr}) = (x_{tr} - x_{opt}) \left(\frac{dy}{dx} \right)_{opt} + y_{opt} \quad (2-7)$$

This scheme is deficient in that dy/dx will have a discontinuity at x_{tr} since P/Q , evaluated at $(x_{tr}, y(x_{tr}))$, will not generally be equal to $(dy/dx)_{opt}$. This difficulty can be avoided if it is possible to rewrite equation (2-1) in an alternative form that does not contain a singularity in the region $x_{opt} \leq x \leq x_{tr}$. In this case, both equations (2-1) (in its alternative form) and (2-6) apply and consequently P/Q , evaluated at $(x_{tr}, y(x_{tr}))$, will equal $(dy/dx)_{opt}$ and no discontinuity occurs. Chapter 3.0 demonstrates how this is accomplished for nozzle-flow calculations.

The foregoing scheme is practical only if $|\alpha - \alpha_{cr}|$ is small. By small we mean that α and α_{cr} agree to three or four significant figures. This is, in fact, a considerable improvement over other saddle-point

methods, which frequently require much greater accuracy for the value of α . The condition that $|\alpha - \alpha_{cr}|$ be small can be satisfied, for example, by requiring that both $|P(x_{opt}, y_{opt})|$ and $|Q(x_{opt}, y_{opt})|$ be small. The numerical calculation can then be fully automated by including provision for restarting the calculation at x_0 when one or both of these conditions is not satisfied. The new calculation would, of course, presumably use a value for α considerably closer to α_{cr} than the preceding one.

An additional advantage of the optimum-point method is that no special choice for the variables is necessary. Furthermore, those equations not containing the saddle-point singularity are not affected.

3.0 APPLICATION TO NONEQUILIBRIUM NOZZLE FLOW

3.1 INTRODUCTORY REMARKS

This chapter applies the optimum-point method to the saddle-point singularity that occurs in steady one-dimensional nozzle flow. For convenience, the discussion will be limited to nonequilibrium nozzle flow, although the method is equally applicable to nonequilibrium diffuser flow and two-phase nozzle or diffuser flow. In addition, the method has been applied successfully to the approximate equilibrium nozzle-flow method given in Part II.

Specifically, this chapter describes how the nonequilibrium nozzle-flow equations can be integrated numerically from an initially subsonic condition to a supersonic one. The same equations and notation, except for the mass flow, given in Part II are retained here. Thus, the quantities x , y and α of Chapter 2.0 become x , distance along the nozzle axis, T , temperature, and m , mass flow, respectively. Equation (2-1) is replaced by

$$\frac{dT}{dx} = \frac{P}{Q}, \quad (3-1)$$

where

$$Q \equiv 1 - M_T^2, \quad (3-2)$$

and

$$P = \frac{u^2}{N_1} \left\{ \frac{1}{A} \frac{dA}{dx} - \phi \right\} \quad (3-3)$$

$$\sum_{i=1}^n c_{F_i} n_i$$

In the foregoing, M_F is the frozen Mach number, u the flow speed, c_{p_i} the specific heat at constant pressure of species i , n_i the mole-mass ratio of species i , N_1 the total number of chemical species, and A the nozzle area. As is evident from definition (3-2), the singularity occurs at $M_F = 1$. At this point P must also be zero if dT/dx is to have a finite value. Consequently, the singularity occurs when simultaneously $M_F = 1$ and $\phi = A^{-1}(dA/dx)$. The quantity ϕ is given by

$$\phi = \frac{1}{\sum_{i=1}^{N_1} n_i} \sum_{i=1}^{N_1} \frac{dn_i}{dx} + \left(\frac{1}{u^2} - \frac{1}{RT \sum_{i=1}^{N_1} n_i} \right) \times \left[\sum_{i=1}^{N_1} (c_{p_i} T + e_{v_i} - e_{D_i}) \frac{dn_i}{dx} + \sum_{i=1}^{N_1} n_i \frac{de_{v_i}}{dx} \right], \quad (3-4)$$

where R is the universal gas constant, e_{v_i} the vibrational energy per mole of species i , and e_{D_i} the energy of reaction per mole of species i . Equations (3-1) through (3-4) constitute only a portion of the system of algebraic and ordinary differential equations that must be solved simultaneously as described in Part II. The other equations, however, are not needed here since only equation (3-1) contains a singularity.

In order to clarify the subsequent discussion, the nozzle is divided, as shown in Figure 2, into five regions. Each region is discussed in turn in the ensuing sections. Region I, discussed in Section 3.2, consists of the low-subsonic portion of the nozzle. (Section 3.2 also considers how an initial estimate for the mass flow can be made.) Region II is similar to region I except that X_{PQ} is now evaluated at each integration step in order to locate the optimum point. Region III begins at the optimum point and terminates when the flow becomes supersonic. Since this region contains the saddle point, an inverted form of equation (3-1) is used here. Region IV "patches" the altered nozzle area actually used in the forward integration in region III to the given nozzle area. Region V includes the remainder of the nozzle. The final section of the chapter, Section 3.7, discusses how the mass flow is modified if a more precise solution is desired.

Three input parameters, denoted by V_i ($i = 1, 2, 3$), are introduced to control certain arbitrary features of the optimum-point method. Thus $x = V_1$ initiates region II, $M_F^* = V_2$ initiates region IV, and V_3 controls the overall accuracy. The quantity V defined as the length of region IV is not to be confused with the input parameters V_i .

3.2 REGION I

The numerical integration of the nonequilibrium nozzle-flow equations starts at x_0 , which for simplicity is taken as zero. At this location, the flow is assumed to be in equilibrium at some density ρ_0 and temperature T_0 . This determines the initial composition $n_{i,0}$ and vibrational energy $e_{v_{i,0}}$. As in Part II, the nozzle area A_0 is considered to be a known function of x .

The mass flow m and stagnation enthalpy h_t , must also be given. The best choice for m , of course, would be the critical mass flow m_{cr} . Although this quantity is unknown, it satisfies the following inequalities (see Bray (1959)):

$$m_{eq} < m_{cr} < m_f,$$

where m_{eq} is the equilibrium-flow value of m and m_f is the frozen-flow value, i.e., the value with all n_i and e_{v_i} held constant at their initial values. Based on experience, a good initial guess for the mass flow is $0.95 m_f$. The frozen mass flow is approximately given by

$$m_f = \left[\left(\frac{2}{\gamma_0 + 1} \right)^{\frac{\gamma_0 + 1}{\gamma_0 - 1}} \gamma_0 R T_0 \sum_{i=1}^{N_1} n_{i,0} \right]^{\frac{1}{2}} \rho_0 A_{th}, \quad (3-5)$$

where A_{th} is the nozzle area at the throat, and the ratio of specific heats γ_0 is given by

$$\gamma_0 = \frac{\sum_{i=1}^{N_1} c_{p_i} n_{i,0}}{\sum_{i=1}^{N_1} (c_{p_i} - R) n_{i,0}}. \quad (3-6)$$

Equation (3-5) is exact when the initial conditions are the stagnation conditions. Since conditions at $x_0 = 0$ correspond to a non-zero frozen Mach number, the value for m_f given by equation (3-5) is somewhat too small. This error is negligible, however, when the frozen Mach number at $x_0 = 0$ is small.

Region I ends when $x = V_1$, where the input parameter V_1 must be chosen sufficiently large that the first minimum of $|X_{PQ}|$ in region II corresponds to the optimum point. Generally V_1 will lie at a nozzle location slightly upstream of the throat.

3.3 REGION II

After each integration step, X_{PQ} is computed and stored for two steps. Its numerical value is given by

$$X_{PQ} = \frac{h}{2} \left[\frac{P + P^+}{P - P^+} - \frac{Q + Q^+}{Q - Q^+} \right], \quad (3-7)$$

where h is the integration step size and $()^+$ denotes the value of $()$ at $x - h$. Equation (3-7) is thus a finite-difference form of equation (2-5). A minimum of $|X_{PQ}|$ occurs when both

$$|X_{PQ}^+| \leq |X_{PQ}^{++}|, \quad |X_{PQ}^+| \leq |X_{PQ}|, \quad (3-8)$$

are satisfied, where X_{PQ}^{++} is the value of X_{PQ} at $x - 2h$. Conditions (3-8) are checked after each integration step in region II. When satisfied, the value of x corresponding to X_{PQ}^+ is the optimum point x_{opt} . At this time, the actual integration is at $x_{opt} + h$. Since region III starts at x_{opt} , it is advisable that the quantities

$$T, dT/dx, \quad n_i (i=1, \dots, N_1), \quad e_{v_i} (i=1, \dots, N_1),$$

be stored for one step in region II.

3.4 REGION III

Region III begins where $x = x_{opt}$ and continues until the frozen Mach number is greater than unity. The temperature T_{III} in this region is given by (see equation (2-6))

$$T_{III} = T_{opt} + (x - x_{opt}) \left(\frac{dT}{dx} \right)_{opt}. \quad (3-9)$$

As pointed out in Chapter 2.0, it is desirable to retain equation (3-1) in region III. This is accomplished by inverting this equation to obtain

$$\frac{dA_{III}}{dx} = A_{III} \left\{ (1 - M_f^2) u^{-2} \left(\sum_{i=1}^{N_1} c_{p_i} n_i \right) \left(\frac{dT}{dx} \right)_{opt} + \phi \right\}. \quad (3-10)$$

In this equation A_{III} is an unknown nozzle area. In region III (and later in region IV) the given nozzle area is denoted by A_g to distinguish it from the nozzle area actually used in the forward integration. These latter nozzle areas are denoted by A_{III} and A_{IV} . In the above form, equation (3-10) contains no singularity.

Equations (3-9) and (3-10) in conjunction with the other nozzle-flow equations yield an exact numerical solution providing A_g is replaced by A_{III} and A_{IV} in regions III and IV. In other words, the mass flow m being used becomes the critical mass flow for a nozzle whose area distribution is the given one in regions I and II and is specified by A_{III} and A_{IV} in regions III and IV. A convenient measure of the accuracy of the optimum-point method that is useful for mass-flow modification discussed in Section 3.7, is thus given by the percent error

$$E \equiv \frac{A_g - A_{III}}{A_g} \times 10^2. \quad (3-11)$$

Region III is terminated when $M_F^2 = V_2$, where the input parameter V_2 is slightly greater than unity (supersonic flow). This nozzle location is referred to as the transfer point x_{tr} .

3.5 REGION IV

At the transfer point, the area A_{III} and its derivative dA_{III}/dx do not equal A_g and dA_g/dx . Consequently, region IV constitutes a short nozzle segment

$$x_{tr} \leq x \leq x_{tr} + V \quad (3-12)$$

that is used to "patch" A_{III} to the given area A_g at $x_{tr} + V$. How the positive quantity V is found is described near the end of this section. Thus, $A_{IV}(x)$ is used to join A_{III} gradually to A_g . The nonequilibrium equations of regions I and II are used here. This section therefore describes a procedure for calculating A_{IV} .

Considerably more effort was expended in this phase than in the rest of this work combined. A satisfactory but sophisticated procedure for finding A_{IV} was arrived at only after an exhaustive search. Any simpler procedure may work for specific stagnation conditions and given nozzle geometry but will prove inadequate for others. Thus, a wide variety of stagnation conditions and given nozzle geometries were used to check the various procedures tried. Only the procedure given here proved to be satisfactory in all cases. For these reasons, the nature of the difficulty will first be described in detail.

At the transfer point, the quantity $A_{III}^{-1}(dA_{III}/dx) - \phi$ in equation (3-3) is close to zero since it is zero just upstream of this point. Inasmuch as $A_{IV}^{-1}(dA_{IV}/dx)$ and $-\phi$ are nearly equal at the start of region IV, a small error in the value of $A_{IV}^{-1}(dA_{IV}/dx)$ will result in a large error in dT/dx . Therefore, unless A_{IV} matches A_{III} at x_{tr} in a smooth fashion, the temperature gradient in region IV will differ drastically from that in region III, i.e., from $(dT/dx)_{opt}$. To avoid this discontinuity the three quantities

$$A, \quad \frac{1}{A} \frac{dA}{dx}, \quad \frac{d}{dx} \left(\frac{1}{A} \frac{dA}{dx} \right), \quad (3-13)$$

are required to be continuous at x_{tr} . These conditions are generally sufficient to assure a smooth variation of T and dT/dx at x_{tr} .

The area function $A^{-1}(dA/dx)$ is the most important of the foregoing quantities since it appears directly in equation (3-1). Its variation with x in the vicinity of the singularity is sketched in Figure 3. In this figure the solid curve represents the given area function $A_g^{-1}(dA_g/dx)$, while the dashed curve labeled III represents $A_{III}^{-1}(dA_{III}/dx)$. The dashed curve corresponds to a mass flow somewhat greater than the critical one since dA_{III}/dx is greater than dA_g/dx . If the mass flow is less than the critical one the dashed curve would be below the solid one. The other curves in Figure 3 are described later.

The continuity requirements (3-13) do not always completely remove the discontinuity in dT/dx at x_{tr} . When Runge-Kutta integration is used (see Part III for further details), an unstable feedback mechanism may occur during the first integration step in region IV. This mechanism operates as follows: As already noted, a small error in the value of $A_{IV}^{-1}(dA_{IV}/dx)$ first results in a larger error in dT/dx . Subsequently, the value of the temperature will be in error and thereby cause errors in the values of dn_i/dx and de_{v_1}/dx . The value of ϕ , given by equation (3-4), therefore will also be somewhat in error. If the errors in the values of $A_{IV}^{-1}(dA_{IV}/dx)$ and ϕ are additive, as is occasionally the case, then the resulting value for dT/dx will now be appreciably in error. This leads to further errors in the values of dn_i/dx , etc.

The above mechanism operates only during the first Runge-Kutta integration step in region IV, no matter how small the size of the integration step. Basically these difficulties are due to the nozzle area not being analytic at x_{tr} . Matching third or higher derivatives of the area at x_{tr} would partially alleviate the problem. This is impractical, however, as will become apparent later. The discontinuity in dT/dx , which is minimized when the procedure described later is used, decays rapidly after the initial integration step in region IV. Thus, by the time three integration steps are completed the temperature gradient has returned to a value consistent with $(dT/dx)_{opt}$.

The feedback difficulty just described is not alleviated by increasing V_2 . Increasing V_2 merely shifts the transfer point x_{tr} downstream and allows the error E to increase further.

It is instructive to describe what happens when a polynomial is used to represent A_{IV} , since this formulation is quite simple. For example, a fifth-degree polynomial in x could be used to match A_{III} , dA_{III}/dx and d^2A_{III}/dx^2 at x_{tr} and the same quantities at $x_{tr} + V$. The resulting variation of $A_{IV}^{-1}(dA_{IV}/dx)$ is sketched in Figure 3 as the dotted curve labeled "polynomial area variation." This curve constitutes a poor approximation to the given one (solid curve) and will result in values for dT/dx considerably different from $(dT/dx)_{opt}$ throughout most of region IV.

As mentioned earlier, when the mass flow is greater than the critical one, A_{III} and dA_{III}/dx at x_{tr} will generally be greater than their corresponding given values. Thus, if A_{IV} is to match A_g at $x_{tr} + V$, then the gradient dA_{IV}/dx must be less than dA_g/dx during part of region IV. This is the reason why any area function $A_{IV}^{-1}(dA_{IV}/dx)$ must cross $A_g^{-1}(dA_g/dx)$ (see Figures 3 and 5). Similar reasoning also leads to the conclusion that the two curves cross when the mass flow is less than the critical one.

We shall now describe the method of formulation and the procedure finally arrived at to determine A_{IV} . The conditions imposed are as follows:

(a) At $x = x_{tr}$, we require that

$$A_{IV} = A_{III}, \quad (3-14)$$

$$\frac{1}{A_{IV}} \frac{dA_{IV}}{dx} = \frac{1}{A_{III}} \frac{dA_{III}}{dx}, \quad (3-15)$$

$$\frac{d}{dx} \left(\frac{1}{A_{IV}} \frac{dA_{IV}}{dx} \right) = \frac{d}{dx} \left(\frac{1}{A_{III}} \frac{dA_{III}}{dx} \right). \quad (3-16)$$

(b) At $x = x_{tr} + V$, we require that

$$A_{IV} = A_g, \quad (3-17)$$

$$\frac{1}{A_{IV}} \frac{dA_{IV}}{dx} = \frac{1}{A_g} \frac{dA_g}{dx}, \quad (3-18)$$

$$\frac{d}{dx} \left(\frac{1}{A_{IV}} \frac{dA_{IV}}{dx} \right) = \frac{d}{dx} \left(\frac{1}{A_g} \frac{dA_g}{dx} \right) . \quad (3-19)$$

- (c) In region IV, we also require that $A_{IV}^{-1}(dA_{IV}/dx)$ be a reasonable approximation to $A_g^{-1}(dA_g/dx)$. This condition will be formulated more precisely later.

In addition to x , the variable \bar{x} is also used, where

$$\bar{x} \equiv \frac{2}{V}(x - x_{tr}) - 1 . \quad (3-20)$$

Equation (3-20) linearly transforms the interval $(x_{tr}, x_{tr}+V)$ into $(-1, 1)$. Since $A_{IV}^{-1}(dA_{IV}/dx)$, rather than A_{IV} , is of primary importance, the following formulation is used:

$$\frac{1}{A_{IV}} \frac{dA_{IV}}{dx} = \lambda_1(\bar{x}) + \frac{1}{A_g} \frac{dA_g}{dx} , \quad (3-21)$$

where A_{IV} and A_g are considered to be functions of x and the function λ_1 is still to be found. To determine A_{IV} , equation (3-21) is integrated from x_{tr} to x , thereby resulting in

$$A_{IV}(x) = \frac{A_{IV}(x_{tr})}{A_g(x_{tr})} A_g(x) \exp[\lambda_2(\bar{x})] , \quad (3-22)$$

where

$$\lambda_2(\bar{x}) \equiv \frac{V}{2} \int_{-1}^{\bar{x}} \lambda_1(\bar{x}) d\bar{x} . \quad (3-23)$$

Condition (3-14) is then satisfied by replacing $A_{IV}(x_{tr})$ in equation (3-22) by the known quantity $A_{III}(x_{tr})$. Condition (3-15) becomes $\lambda_1(-1) = \eta_1$, where the known constant η_1 is given by (see Figure 3)

$$\eta_1 = \left[\frac{1}{A_{III}} \frac{dA_{III}}{dx} - \frac{1}{A_g} \frac{dA_g}{dx} \right]_{x=x_{tr}} . \quad (3-24)$$

$$\eta_3 = -\frac{15}{16} \left[\frac{2}{V} \ln \left(\frac{A_{III}}{A_g} \right)_{x=x_{tr}} + \eta_1 + \frac{1}{3} \eta_2 \right] . \quad (3-31)$$

The foregoing results satisfy conditions (a) and (b) given by equations (3-14) through (3-19). Condition (c) is approximately satisfied by choosing f_3 appropriately. For simplicity, it is taken as

$$f_3(\bar{x}) = \eta_4 \bar{x} , \quad (3-32)$$

where the constant η_4 is still to be determined.

Figure 3 shows a sketch designated by (IV) of $A_{IV}^{-1}(dA_{IV}/dx)$ for a positive value of η_1 , while Figure 4 shows the corresponding λ_1/η_1 curve. Figure 5 is similar to Figure 3 except that η_1 is negative. In either case, λ_1 has an extremum in the vicinity of the origin. This extremum and its location are designated by λ_1^* and \bar{x}^* . As is evident from Figures 3 and 4, condition (c) is approximately fulfilled if $|\lambda_1^*|$ is minimized.

For fixed values of η_1 , η_2 , and η_3 , \bar{x}^* is determined by the condition

$$\frac{\partial \lambda_1}{\partial \bar{x}} = 0 , \quad (3-33a)$$

or

$$\eta_4 = \frac{3}{4} \eta_1 + \frac{1}{4} \eta_2 \left(\frac{1 + 3\bar{x}^*}{1 + \bar{x}^*} \right) + \bar{x}^* (4\eta_3 + 5\eta_4 \bar{x}^*) . \quad (3-33b)$$

To minimize $|\lambda_1^*|$, we first note that $\lambda_1^* = \lambda_1(\bar{x}^*(\eta_4); \eta_4)$. Hence, the desired minimum occurs when

$$\frac{d\lambda_1^*}{d\eta_4} = \left(\frac{\partial \lambda_1}{\partial \eta_4} \right)_{\bar{x}=\bar{x}^*} + \left(\frac{\partial \lambda_1}{\partial \bar{x}} \right)_{\bar{x}=\bar{x}^*} \left(\frac{d\bar{x}^*}{d\eta_4} \right) = 0 . \quad (3-34a)$$

The second term on the right-hand side, however, is zero by virtue of equation (3-33a). Thus, equation (3-34a) can be shown to reduce to

$$(\bar{x}^* + 1)^2 (\bar{x}^* - 1)^2 \bar{x}^* = 0 . \quad (3-34b)$$

The solution of equations (3-33b) and (3-34b) readily results in

$$\bar{x}^* = 0, \quad \eta_4 = \frac{3}{4} \eta_1 + \frac{1}{4} \eta_2. \quad (3-35)$$

When equations (3-28) through (3-32) and equations (3-35) are combined, the following is obtained:

$$-\frac{\lambda_1^*}{\eta_1} = \frac{7}{16} + \frac{15}{8} \left(\frac{1}{\eta_1 V} \right) \ln \left[\frac{A_{III}}{A_g} \right]_{x=x_{tr}} + \frac{1}{16} \frac{\eta_2}{\eta_1}. \quad (3-36)$$

The parameter V is now determined by setting $-(\lambda_1^*/\eta_1) = (3/4)$ in equation (3-36) where, for convenience, the term $\eta_2/(16\eta_1)$ is neglected. When examined a posteriori, the value of this term is indeed found to be small compared with unity. Thus, V is given by

$$V = \frac{6}{\eta_1} \ln \left[\frac{A_{III}}{A_g} \right]_{x=x_{tr}}. \quad (3-37)$$

A smaller value than $3/4$ for $-(\lambda_1^*/\eta_1)$ would result in a larger value for V , while a larger value than $3/4$ would result in a smaller V . The choice made here, however, proved to be an acceptable one. As a consequence of equation (3-37), the constant η_3 is given by

$$\eta_3 = -\frac{5}{4} \eta_1 - \frac{5}{16} \eta_2. \quad (3-38)$$

The pertinent equations of this section are summarized in a form suitable for numerical work in Appendix I.

3.6 REGION V

This region includes the remainder of the nozzle. The given nozzle area is used, and the forward integration proceeds as described in Part II.

3.7 MASS-FLOW MODIFICATION

The initial value for the mass flow when chosen according to the method in Section 3.2 may differ by as much as 5% from the critical mass flow. To obtain a more precise calculation, a method is now described for modifying the mass flow and the stagnation enthalpy.

After each integration step in region III the following check is performed:

$$|E| \leq V_3, \quad (3-39)$$

where E is defined by equation (3-11) and V_3 is a positive input parameter that controls the accuracy of the method. As long as condition (3-39) is satisfied, the integration proceeds as described in Section 3.4. If condition (3-39) is not satisfied, then the integration starts over again at $x_0 = 0$ with new values for the mass flow and stagnation enthalpy.

To determine a new value for the mass flow that is closer than the preceding one to the critical mass flow, two different fictitious frozen flows are compared. The first flow uses the current mass flow m_a , the temperature and nozzle area at $x_0 = 0$, and the temperature and nozzle area at the point in region III where (3-39) is not satisfied. According to the usual frozen-flow equations, m_a is given by

$$m_a = c_0 \left[\frac{1 - \frac{T_{III}}{T_0}}{\left(\frac{A_0}{A_{III}} \right)^2 \left(\frac{T_0}{T_{III}} \right)^{\frac{\gamma_0 - 1}{\gamma_0}} - 1} \right]^{\frac{1}{2}}, \quad (3-40)$$

where γ_0 is defined by equation (3-6) and the constant c_0 is

$$c_0 \equiv \left[\left(\frac{2\gamma_0}{\gamma_0 - 1} \right) RT_0 \sum_{i=1}^{N_1} n_{i,0} \right]^{\frac{1}{2}} \rho_0 A_0. \quad (3-41)$$

The second flow is similar to the first except that the improved mass flow m_b replaces m_a and the value of A_g at the point where (3-39) is not satisfied replaces A_{III} . Thus m_b is given by

$$m_b = c_0 \left[\frac{1 - \frac{T_{III}}{T_0}}{\left(\frac{A_0}{A_{III}} \right)^2 \left(\frac{T_0}{T_{III}} \right)^{\frac{\gamma_0 - 1}{\gamma_0}} - 1} \right]^{\frac{1}{2}}. \quad (3-42)$$

Taking the ratio of equations (3-40) and (3-42) then results in the desired mass-flow correction formula

$$m_b = \left[\frac{\frac{2}{\gamma_o - 1} \left(\frac{T_o}{T_{III}} \right) - \left(\frac{A_{III}}{A_o} \right)^2}{\frac{2}{\gamma_o - 1} - \left(\frac{A_g}{A_o} \right)^2} \right]^{\frac{1}{2}} \left(\frac{A_g}{A_{III}} \right) m_a \quad (3-43)$$

The stagnation enthalpy h_t is also modified in order that the new nozzle-flow solution can start at the same equilibrium state previously used. Thus, ρ_o , T_o , $n_{i,o}$, and $e_{v_{i,o}}$ remain unchanged. This is readily accomplished providing ρ_o is unchanged, since the other quantities are initial conditions. The requirement

$$\rho_o = \frac{m_a}{A_o (u_o)_a} = \frac{m_b}{A_o (u_o)_b} \quad (3-44)$$

is therefore imposed, where $(u_o)_a$ is the flow speed at $x_o = 0$ when the mass flow is m_a and $(u_o)_b$ is the corresponding flow speed when the mass flow is m_b . The energy equation is now evaluated at $x_o = 0$ for flows (a) and (b) as follows:

$$(h_t)_a = h_o + \frac{1}{2} (u_o)_a^2, \quad (3-45a)$$

$$(h_t)_b = h_o + \frac{1}{2} (u_o)_b^2, \quad (3-45b)$$

where h_o is the enthalpy at $x_o = 0$. By combination of equations (3-44) and (3-45), the desired stagnation-enthalpy correction formula is obtained as

$$(h_t)_b = (h_t)_a + \frac{1}{2} \left(\frac{m_a}{\rho_o A_o} \right)^2 \left[\left(\frac{m_b}{m_a} \right)^2 - 1 \right]. \quad (3-46)$$

4.0 RESULTS AND DISCUSSION

4.1 GIVEN CONDITIONS

This chapter describes the results of one nonequilibrium nozzle-flow calculation that utilized the foregoing optimum-point method. This calculation and all others that were performed are based on the same gas model used in Parts I and II. This is a model of air consisting of the five species O , N , NO , N_2 , and O_2 (identified by subscripts $i = 1, \dots, 5$, respectively). The same eight reactions and the same rate constants are also retained.

The variation of nozzle area with distance for all five regions is given by

$$A_g = 10 - 6x + x^2. \quad (4-1)$$

This equation represents a hyperbolic nozzle with a throat area of 1 cm^2 located at $x = 3.0 \text{ cm}$. All numerical integrations started at $x = 0 \text{ cm}$ where the area is 10 cm^2 and concluded at $x = 4 \text{ cm}$ where the supersonic flow is well into region V.

At the initial point $x = 0 \text{ cm}$ the flow is assumed to be in equilibrium at a temperature of 8000°K and a density of $2.80 \times 10^{-5} \text{ gm/cm}^3$. These conditions were chosen so that a significant portion of the diatomic species would be dissociated at $x = 0$. In addition, to insure that the flow would depart from equilibrium upstream of the throat, a small initial density as compared with that used in Parts I and II was necessary. For all practical purposes, the foregoing are also the stagnation conditions since the initial frozen Mach number is 0.0548. The equilibrium composition and vibrational energies corresponding to this density and temperature are given in the following table:

EQUILIBRIUM COMPOSITION AND VIBRATIONAL ENERGIES
FOR AIR AT 8000°K AND $2.80 \times 10^{-5} \text{ GM/CM}^3$

i	SPECIES	n_i (MOLES/GM)	e_{v_i} (DYNE CM/MOLE)
1	O	$.14598473 \times 10^{-1}$	-
2	N	$.45508697 \times 10^{-1}$	-
3	NO	$.60071580 \times 10^{-4}$	$.55920669 \times 10^{12}$
4	N_2	$.45156159 \times 10^{-2}$	$.53593265 \times 10^{12}$
5	O_2	$.72687672 \times 10^{-6}$	$.57674503 \times 10^{12}$

Initial values for the mass flow and stagnation enthalpy were chosen in accord with the discussion in Chapter 3. The final values for these quantities are given in the next section. The following values were used for the input parameters V_1 :

$$V_1 = 2.8 ,$$

$$V_2 = 1.01 ,$$

$$V_3 = 0.5 .$$

The optimum-point method was also used in conjunction with the approximate equilibrium formulation given in Part II and modified in Appendix II of this report. The same nozzle geometry and initial conditions as described above were used (except for mass flow and stagnation enthalpy). The only changes were that the n_i were sequenced as follows: O_2 , N, NO, N_2 , O . The reason for this change is discussed in Appendix II. In addition, for reasons given in the next section, a value of 1.0 was used for V_3 .

The calculations presented here were chosen because they proved to be the most troublesome in terms of the instability described in Section 3.5. In fact, of the many procedures for determining A_{IV} that were tried only the one given here dealt successfully with this case. In terms of instability, the approximate equilibrium calculation was more troublesome than the nonequilibrium one. This point is discussed further in Section 4.2.

4.2 RESULTS OF THE OPTIMUM-POINT METHOD

On the basis of equation (3-5), the foregoing conditions result in a frozen mass flow of 4.1925 gm/sec. Although equation (3.5) is approximate, this value is very close to the true value since the initial Mach number is nearly zero. The initial value for the nonequilibrium mass flow was therefore chosen to be $0.95 \times 4.1925 = 3.98$ gm/sec. The final values for the mass flow and stagnation enthalpy came out to be 4.0540000 gm/sec and 7.0064822×10^{10} cm²/sec², respectively. Figures 5 through 11 are based on these nonequilibrium values. This value for the mass flow is slightly below the critical one, as is evident from Figure 5. A subsequent calculation with a mass flow of 4.0830000 gm/sec showed that this larger value was, in comparison, well above the critical one. Thus, the mass-flow value of 4.054 gm/sec is accurate at least to three significant figures.

With regard to accuracy, let us first compare the location and area of the throat for the two nozzle areas, A_g and A_{III} . This comparison is presented in the following table:

LOCATION AND AREA OF THE NOZZLE THROAT

<u>NOZZLE AREA</u>	<u>THROAT LOCATION</u>	<u>THROAT AREA</u>
A_g	3.0000 cm	1.00000 cm^2
A_{III}	3.0083 cm	0.99937 cm^2

Another pertinent quantity is the maximum value of the percent error E . This occurs at x_{tr} and is 0.217%, well below its upper limit V_3 of 0.5%. Finally, we note that the calculated area function $A^{-1}(dA/dx)$, shown in Figure 5, differs but slightly from the corresponding given area function in both regions III and IV. (See Figure 3 for a more detailed description of the curves in Figure 5.) We therefore conclude that A_{III} and A_{IV} do not differ significantly from A_g for reasonably accurate values of the mass flow, i.e., three significant figures. Calculations based on a more accurate estimate for the mass flow than 4.054 gm/sec could be readily obtained. Such a calculation, however, was not deemed necessary since the results for 4.054 gm/sec and 4.083 gm/sec differed only negligibly. Thus, when the optimum-point method is used the resulting solution differs negligibly from the critical one for reasonably accurate values of the mass flow.

For the approximate equilibrium calculation, the values for mass flow and stagnation enthalpy are 3.7268000 gm/sec and $7.0048583 \times 10^{10} \text{ cm}^2/\text{sec}^2$, respectively. This calculation, which is also shown in Figures 6 through 11, differed from the nonequilibrium one in two respects. First, greater accuracy was required for the mass-flow value. This is basically a consequence of the curves for $P = 0$ and $Q = 0$ being close together upstream of the saddle point. As a result, for any value of the mass flow different from the critical one, the calculation behaves as if the singularity were located at the geometric throat, where the equilibrium Mach number is unity, rather than at $M_f = 1$. The extent of region III is therefore somewhat longer and the percent error at the transfer point is larger as compared with the nonequilibrium calculation. Hence, a larger value was used for V_3 in the equilibrium calculation. As in the nonequilibrium case, however, the solution for slightly different values of the mass flow (i.e., $m = 3.7271 \text{ gm/sec}$) differed negligibly from the one given here. Thus, the mass-flow value of 3.7268 gm/sec is accurate to at least four significant figures.

The second difference is that the instability at the start of region IV is more pronounced for the equilibrium calculation. This resulted in a reduction in the integration step size at the start of region IV. Since the instability decays rapidly, however, the step size then proceeds to increase to its former level.

4.3 GASDYNAMIC RESULTS

Figures 6 through 11 show the results of the nonequilibrium and equilibrium calculations. In all the figures the abscissa is the distance along the nozzle axis.

Figure 6 shows the temperature variation. For interest the temperature variation is also shown for a flow frozen at the same initial conditions. From this figure it is evident that the nonequilibrium solution starts to diverge from the equilibrium one at about $x = 1.8$ cm, where the frozen Mach number is 0.234. Along the entire nozzle, the nonequilibrium and frozen-flow temperatures are quite close, indicating that once the flow diverges from the equilibrium one it freezes rapidly. This result is not a general one but rather is a consequence of the specific stagnation conditions and nozzle geometry used for these calculations. In particular, a rapidly varying nozzle geometry, which is the case here, tends to favor rapid freezing. The large difference between the equilibrium and nonequilibrium temperature after $x = 2$ cm is due to nitrogen recombination in the equilibrium flow. This recombination is briefly discussed later.

Figure 7 shows the density and pressure variations. In comparison with Figure 6, it is seen that density and pressure are not as sensitive as the temperature to nonequilibrium effects. This result is in accord with other nozzle-flow calculations, such as those of Bray (1959).

Figure 8 shows the variation of the flow-speed. The equilibrium and nonequilibrium speeds differ slightly at $x = 0$ cm because the respective mass flows are different. Figures 9 and 10 show the variation of chemical composition and vibrational energy, respectively.

All quantities shown in Figures 6 through 10, with the exception of flow-speed, are nearly constant in the region from $x = 0$ cm to $x = 1.8$ cm. In this low-subsonic region, the nonequilibrium (or equilibrium) solution is given approximately by

$$uA = \frac{\dot{m}}{\rho} = \text{constant}, \quad (4-2)$$

where all other variables are constant. Thus, the nonequilibrium and equilibrium solutions will be close here regardless of the values of the chemical and vibrational relaxation lengths. In this region, all relaxation lengths are directly proportional to velocity and therefore increase steadily. Should any of the characteristic lengths become sufficiently large here, the flow will then start to diverge from equilibrium as soon as compressibility becomes important. This occurred in the calculation shown here.

Approximate values for the characteristic lengths at $x = 0$ cm and at $x = 1.8$ cm were calculated according to the theory in Part II and in Appendix II. They are presented in the following table:

CHEMICAL AND VIBRATIONAL CHARACTERISTIC LENGTHS

RATE EQUATION FOR	CHARACTERISTIC LENGTH, CM, AT $x = 0$ cm	CHARACTERISTIC LENGTH, CM, AT $x = 1.8$ cm
O , CHEMICAL	1.32×10^{-3}	5.40×10^{-3}
N , "	6.71×10^{-2}	2.74×10^{-1}
NO , "	5.07×10^{-4}	2.07×10^{-3}
NO , VIBRATIONAL	1.30×10^{-3}	5.32×10^{-3}
N ₂ , "	1.59×10^{-2}	6.50×10^{-2}
O ₂ , "	1.11×10^{-3}	4.55×10^{-3}

At $x = 0$ cm all of the characteristic lengths are small. At $x = 1.8$ cm, however, the mole-mass ratio for atomic nitrogen should start to diverge from its equilibrium value, whereas the mole-mass ratios for atomic oxygen and nitric oxide are still close to their equilibrium values. Since the mole-mass ratios for diatomic nitrogen and diatomic oxygen are given by the equations for conservation of components, the former will also start to diverge from equilibrium while the latter will not.

The preceding conclusions are not discernible from Figure 9. Indeed, this figure indicates that nitric oxide is the first species to diverge from equilibrium and that atomic nitrogen remains close to its equilibrium value until $x = 3.0$ cm. These fallacious conclusions are a direct result of the log scale used for the chemical composition, a convenient and common practice. To clarify the situation, the variation of $|n_i - n_{i,eq}|$ is shown in Figure 11, where $n_{i,eq}$ is the mole-mass ratio of species i for the equilibrium-flow solution. This figure clearly shows that the mole-mass ratios for atomic and diatomic nitrogen diverge from their equilibrium-flow value far more appreciably than do those for the other species. Figure 11 is thus in accord with the findings based on the characteristic lengths. The valley in the curve for diatomic oxygen in Figure 11 is due to the equilibrium and non-equilibrium mole-mass ratios crossing, as shown in Figure 9.

According to the foregoing table of characteristic lengths, the vibrational energy of nitric oxide will diverge from its local equilibrium value upstream of the other vibrational energies. Thus Figure 10, while correct, cannot be used to determine how close any vibrational energy is to its local-equilibrium value. This situation has been

discussed in detail in Part II.

Figure 9 shows that a significant amount of nitrogen recombination occurs in the equilibrium-flow solution. This recombination accounts for the large difference between the equilibrium and nonequilibrium temperatures. In the equilibrium calculation, the mole-mass ratios for the other species, i.e., O , O_2 , and NO , remain fairly constant. This is due to the small decrease in the equilibrium temperature, which favors recombination, being counterbalanced by the large decrease in the equilibrium density, which favors dissociation.

REFERENCES

- Bray, K. N. C., 1959, "Atomic Recombination in a Hypersonic Wind-Tunnel Nozzle". J. Fluid Mech., Vol.6, Part 1, p.1.
- Belotserkovskii, O. M., 1957, "Flow Past a Circular Cylinder with a Detached Shock Wave". Dokl. Akad. Nauk., Vol.113, No.3.
- Belotserkovskii, O. M., 1958, "Flow with a Detached Shock Wave about a Symmetrical Profile". Appl. Math. and Mech., Vol.22, p.279.
- Emanuel, G., and Vincenti, W. G., 1962, "Method for Calculation of the One-Dimensional Nonequilibrium Flow of a General Gas Mixture through a Hypersonic Nozzle". AEDC-TDR-62-131.
- Emanuel, G., 1963, "Problems Underlying the Numerical Integration of the Chemical and Vibrational Rate Equations in a Near-Equilibrium Flow". AEDC-TDR-63-82.
- Eschenroeder, A. Q., Boyer, D. W., and Hall, G. J., 1962, "Nonequilibrium Expansions of Air with Coupled Chemical Reactions". Phys. Fluids, Vol.5, No.5, p.615.
- Glauz, R. D., 1962, "Combined Subsonic-Supersonic Gas-Particle Flow". ARS Jour., Vol.32, No.5, p.773.
- Reichenbach, R., 1960, "Combustion Research". Ph.D. Diss., Calif. Inst. of Tech.
- Vincenti, W. G., 1961, "Calculations of the One-Dimensional Nonequilibrium Flow of Air through a Hypersonic Nozzle - Interim Report". AEDC-TN-61-65.
- Xerikos, J., and Anderson, W. A., 1962, "A Critical Study of the Direct Blunt Body Integral Method". Douglas Aircraft Rept. SM-42603.

APPENDIX I

ANALYTICAL EXPRESSIONS FOR $A_{IV}(x)$

The variation of nozzle area with distance in region IV is given below. At the start of this region the parameters η_1^+ , η_1 , V , and η_2 are calculated. Equations (I-5) through (I-9) then determine A_{IV} and dA_{IV}/dx .

$$\eta_1^+ = \left[\frac{1}{A_{III}} \frac{dA_{III}}{dx} - \frac{1}{A_g} \frac{dA_g}{dx} \right]_{x=x_{tr}-h} \quad (I-1)$$

$$\eta_1 = \left[\frac{1}{A_{III}} \frac{dA_{III}}{dx} - \frac{1}{A_g} \frac{dA_g}{dx} \right]_{x=x_{tr}} \quad (I-2)$$

$$V = \frac{6}{\eta_1} \ln \left[A_{III}/A_g \right]_{x=x_{tr}} \quad (I-3)$$

$$\eta_2 = \frac{V}{2h} (\eta_1 - \eta_1^+) \quad (I-4)$$

$$\bar{x} = \frac{2}{V} (x - x_{tr}) - 1 \quad (I-5)$$

$$\lambda_1(\bar{x}) = \left(\frac{\bar{x}-1}{4} \right)^2 \left[4(3\bar{x}^3 + \bar{x}^2 - 6\bar{x} - 3)\eta_1 + (\bar{x}+1)(4\bar{x}^2 - \bar{x} - 1)\eta_2 \right] \quad (I-6)$$

$$\lambda_2(\bar{x}) = \frac{V}{96} (\bar{x}+1) \left[(6\bar{x}^5 - 18\bar{x}^4 + 3\bar{x}^3 + 37\bar{x}^2 - 37\bar{x} + 1)\eta_1 + (\bar{x}+1)(2\bar{x}-1)(\bar{x}-1)^3\eta_2 \right] \quad (I-7)$$

$$A_{IV}(x) = \left[A_{III}/A_g \right]_{x=x_{tr}} A_g(x) \exp \left[\lambda_2(\bar{x}) \right] \quad (I-8)$$

$$\frac{dA_{IV}}{dx} = A_{IV} \left[\lambda_1(\bar{x}) + \frac{1}{A_g(x)} \frac{dA_g}{dx} \right] \quad (I-9)$$

APPENDIX II

MODIFICATION OF THE APPROXIMATE EQUILIBRIUM METHOD OF PART II

Two modifications of the approximate equilibrium method of Part II are given here. The need for these changes became apparent when equilibrium nozzle-flow solutions were sought that required the optimum-point method. Once these changes were incorporated, along with the condition that $\beta_{ii} - \alpha_{ii} \neq 0$ ($i = 1, \dots, N_3$) as explained in Part II, no further difficulties were encountered. (See Part II for definition of symbols.)

The first change requires that $\tilde{\gamma}$ be replaced by $-\tilde{\gamma}_i$ in equation (34c) of Part II as follows:

$$\frac{dn_i}{dx} = \tilde{\gamma}_i n_i [1 - \tilde{L}_i], \quad i = 1, \dots, N_3, \quad (\text{II-1})$$

where the $|\tilde{\gamma}_i|$ are large constants. To understand the reason for this change, we first derive the characteristic lengths ϵ_{ci} for equations (II-1). The derivation is explained in detail in Appendix III of Part II. Thus, the ϵ_{ci} are given by

$$\epsilon_{ci}^{-1} = -\frac{\partial F_i}{\partial n_i}, \quad i = 1, \dots, N_3, \quad (\text{II-2})$$

with density, temperature, and all n_j except n_i held fixed. The quantity F_i is defined by

$$F_i = \tilde{\gamma}_i n_i [1 - \tilde{L}_i], \quad i = 1, \dots, N_3. \quad (\text{II-3})$$

When the characteristic lengths ϵ_{ci} are defined as above (i.e., without absolute value signs and with density held fixed), they are equivalent to u/κ_{ii} given in Part III. After the partial differentiation is performed, and conservation of components as well as $\tilde{L}_i \cong 1$ (law of mass action) are accounted for, we obtain

$$\epsilon_{ci} = + \frac{1}{\tilde{\gamma}_i \tilde{\alpha}_{ii} + \sum_{k=N_3+1}^{N_1} a_{ki} \tilde{\alpha}_{ik} \left(\frac{n_i}{n_k} \right)}, \quad i = 1, \dots, N_3. \quad (\text{II-4})$$

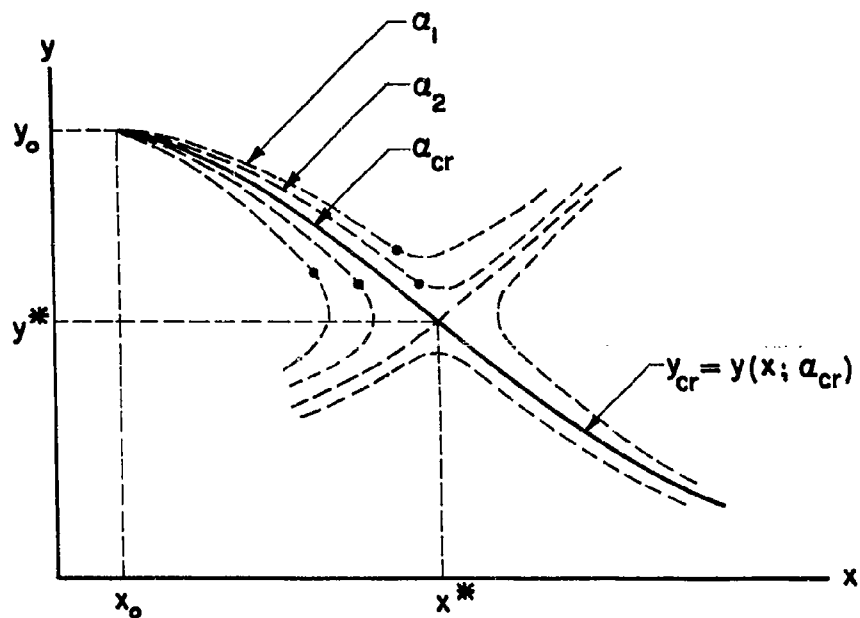


Fig. 1 Integral Curves of $(dy/dx) = (P/Q)$

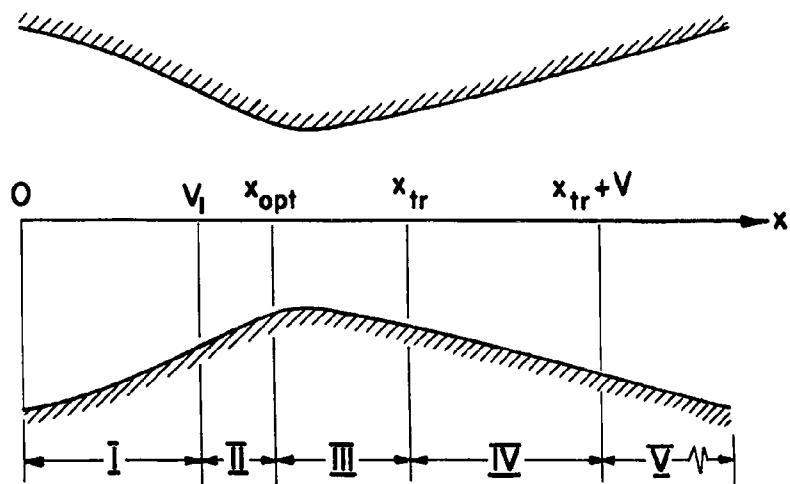


Fig. 2 Sketch of Nozzle Configuration

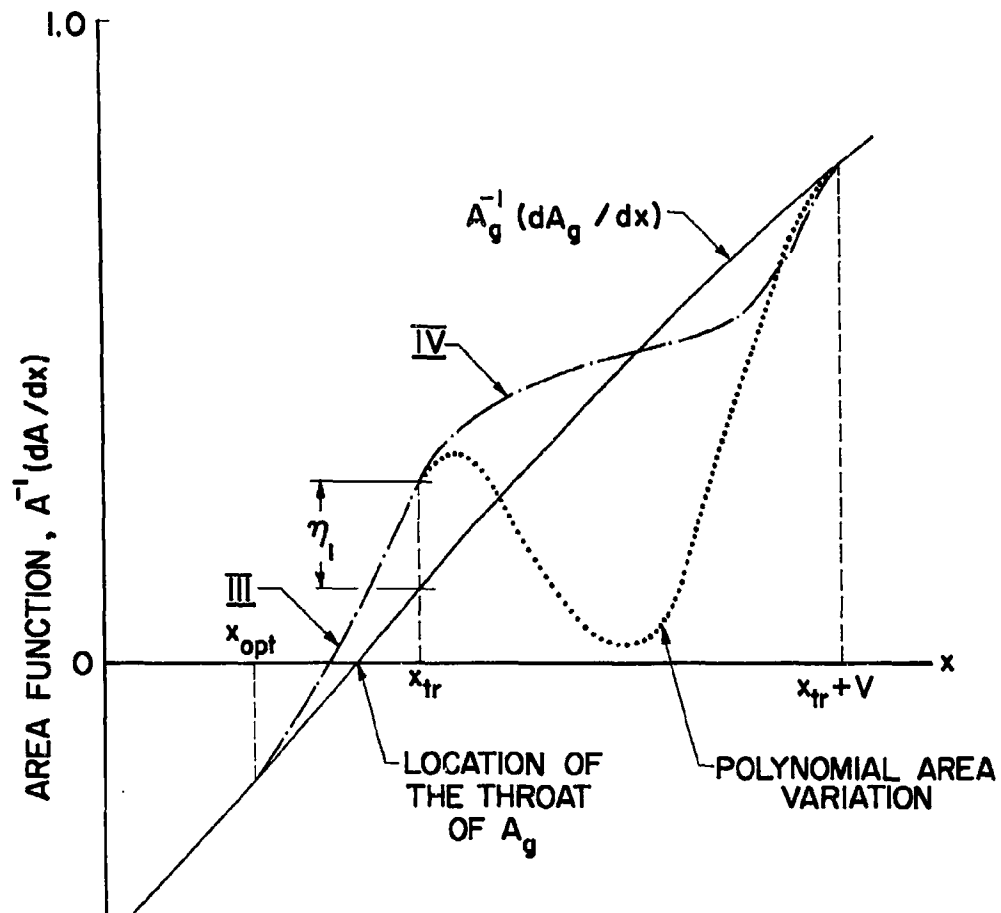
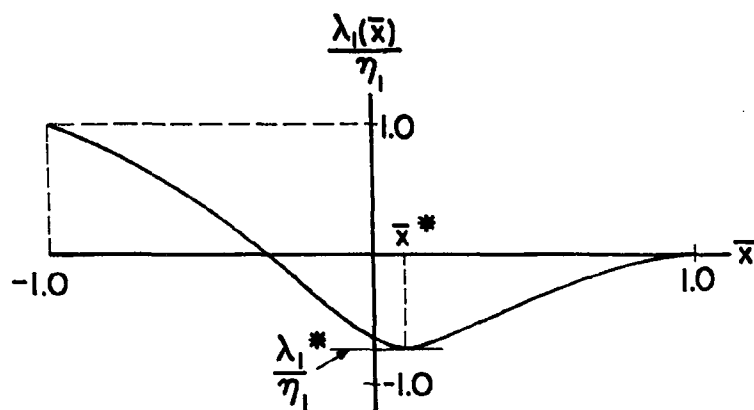
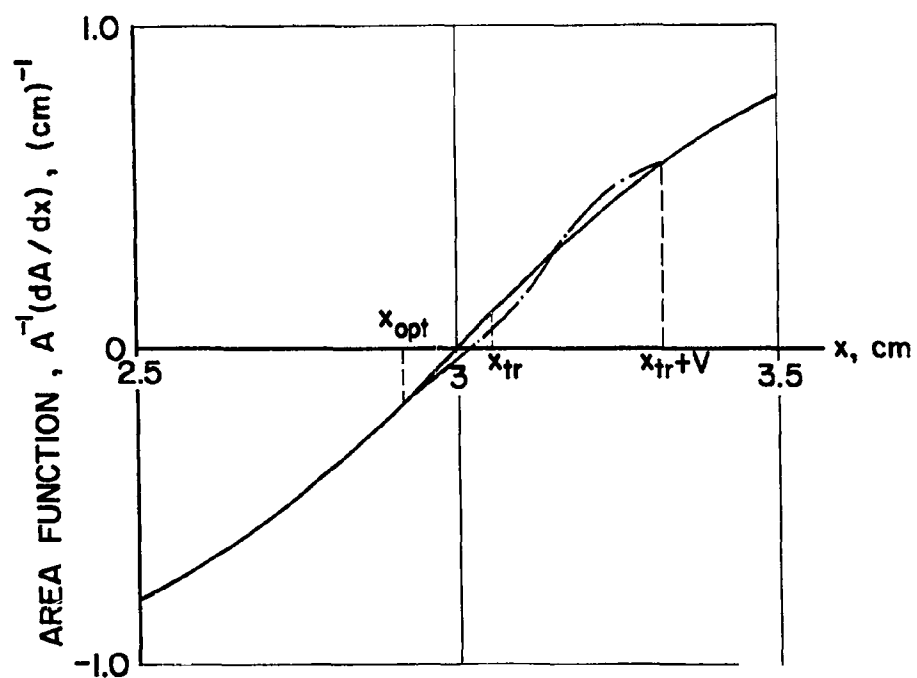


Fig. 3 Sketch of the Area Function $A^{-1}(dA/dx)$

Fig. 4 Sketch of $\lambda_1(\bar{x})/\eta_1$ Fig. 5 Area Function $A^{-1}(dA/dx)$

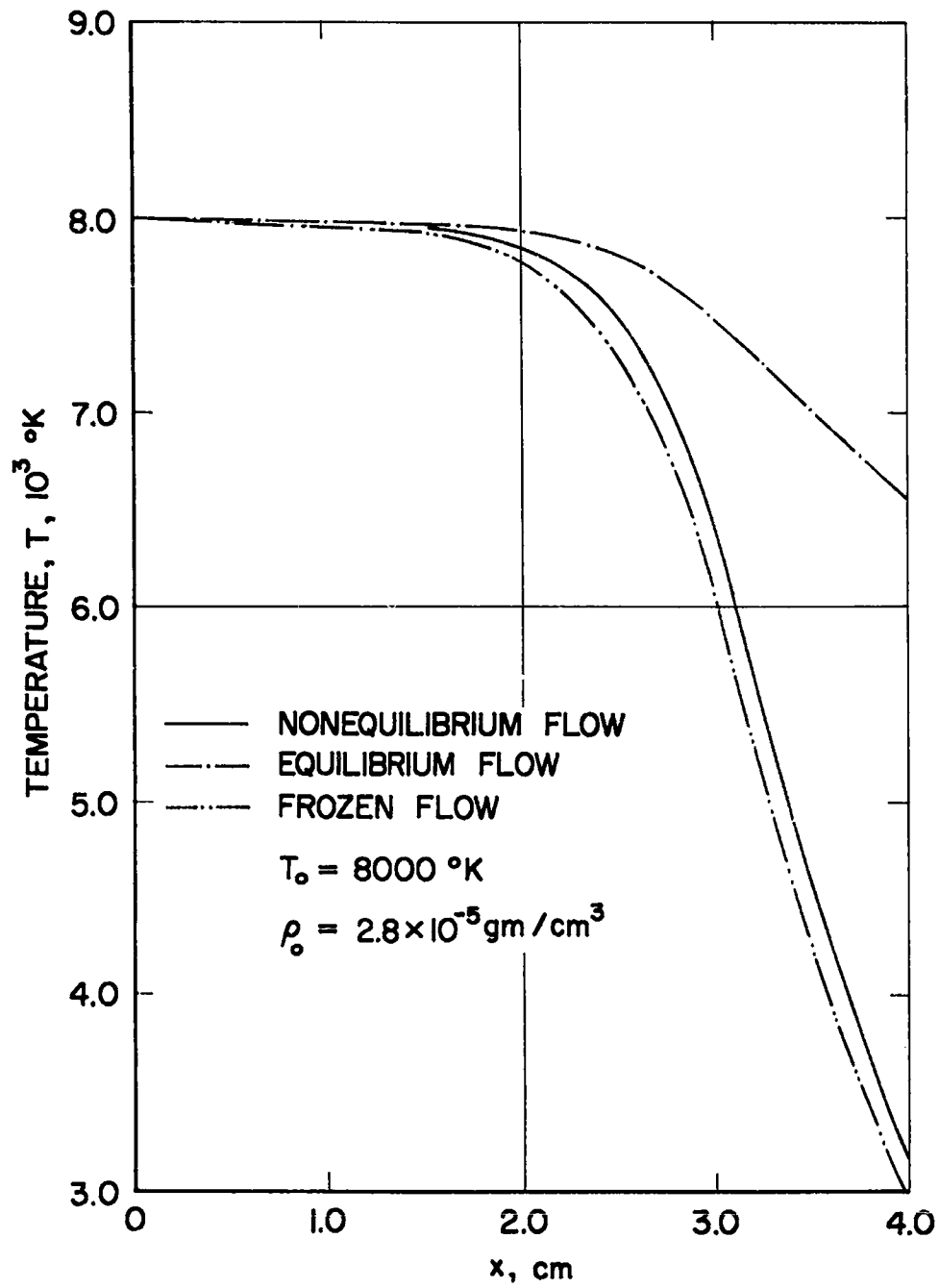


Fig. 6 Temperature

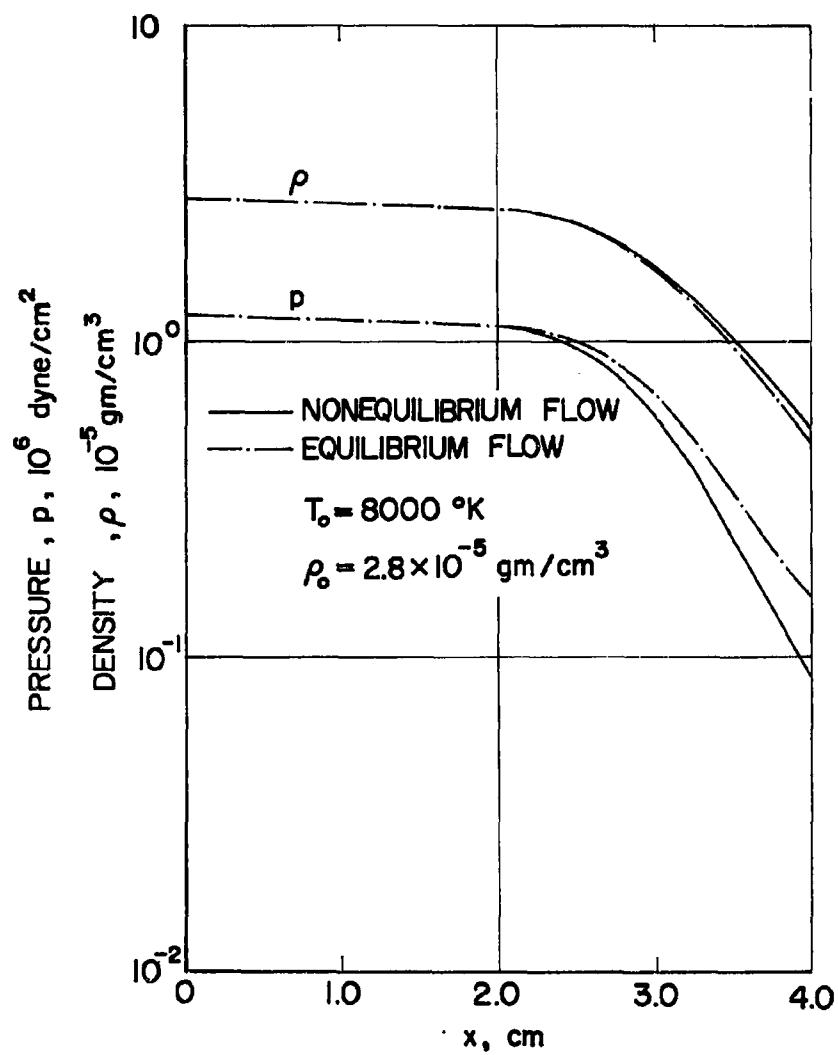


Fig. 7 Pressure and Density

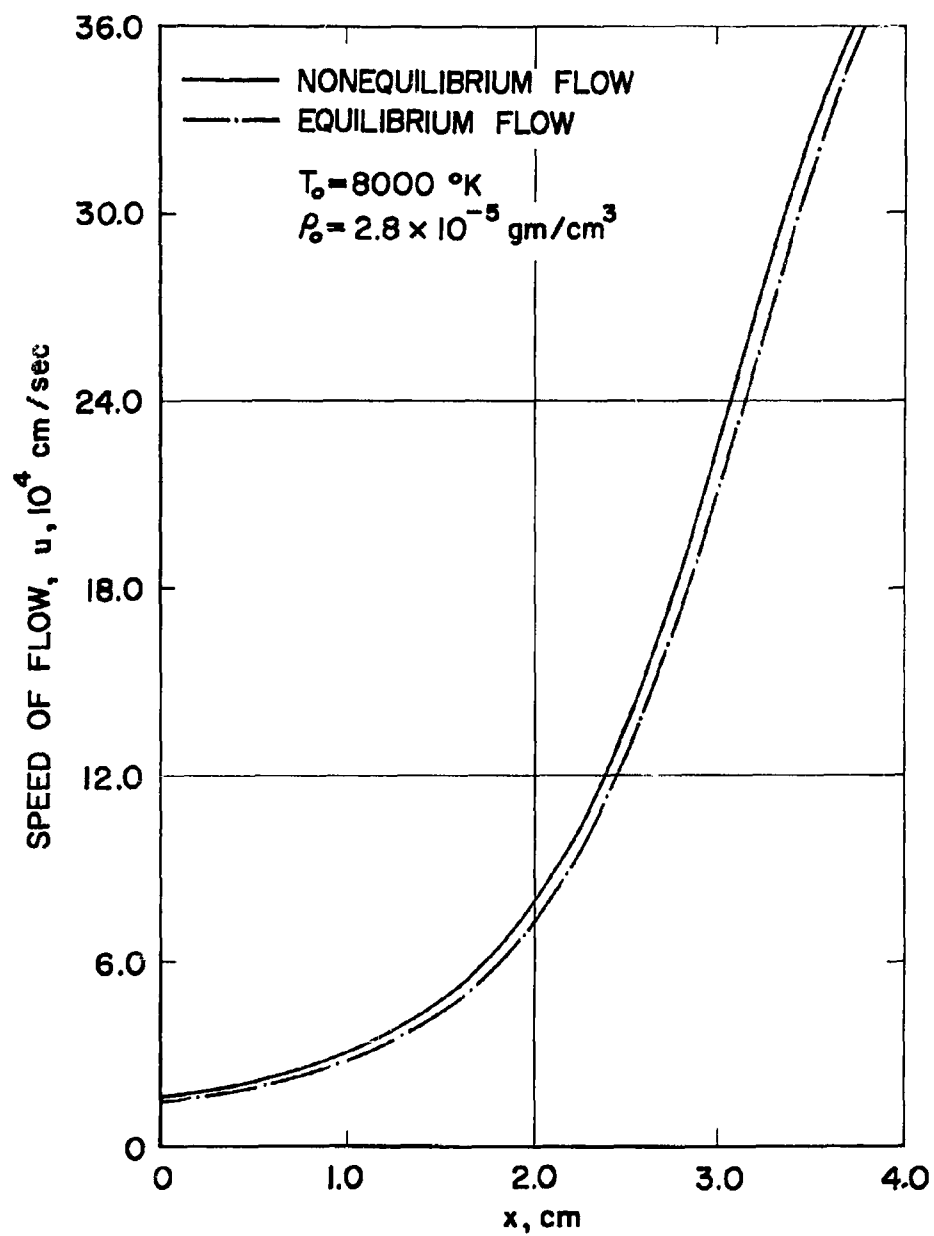


Fig. 8 Speed of Flow

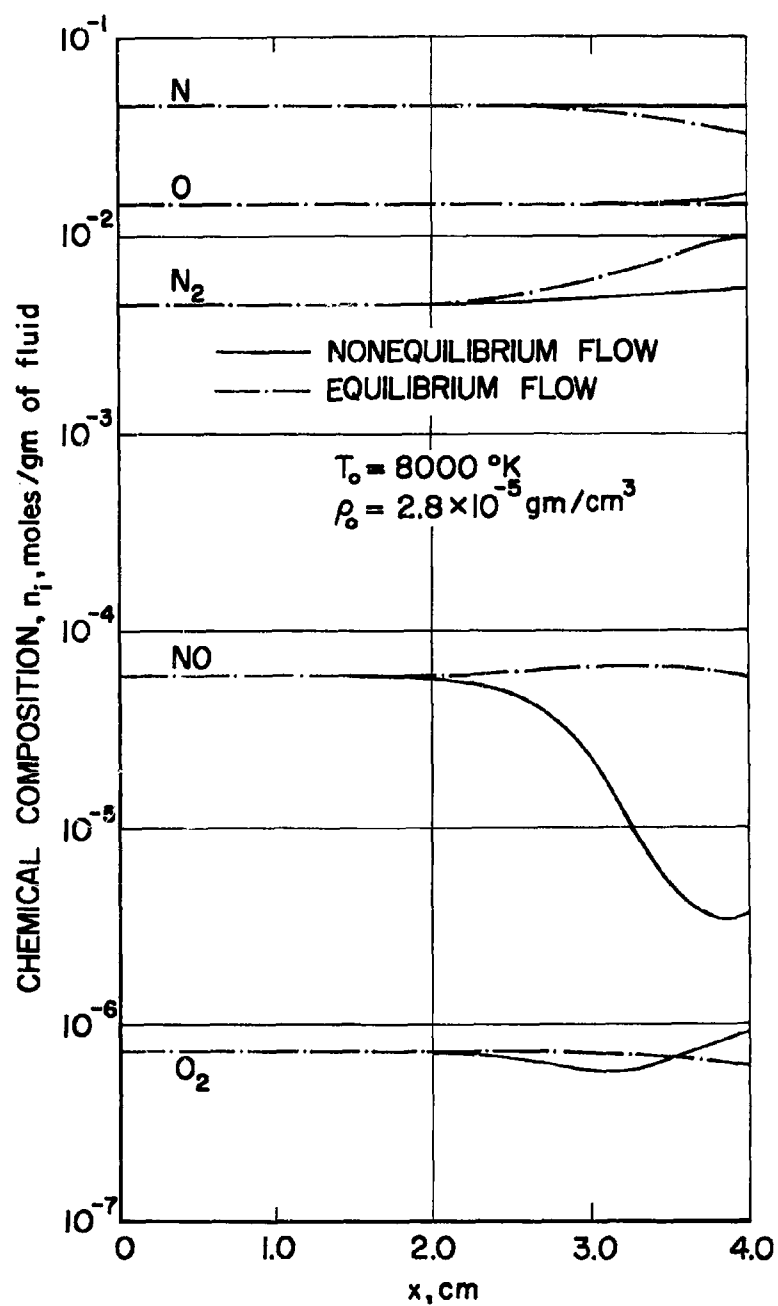


Fig. 9 Chemical Composition

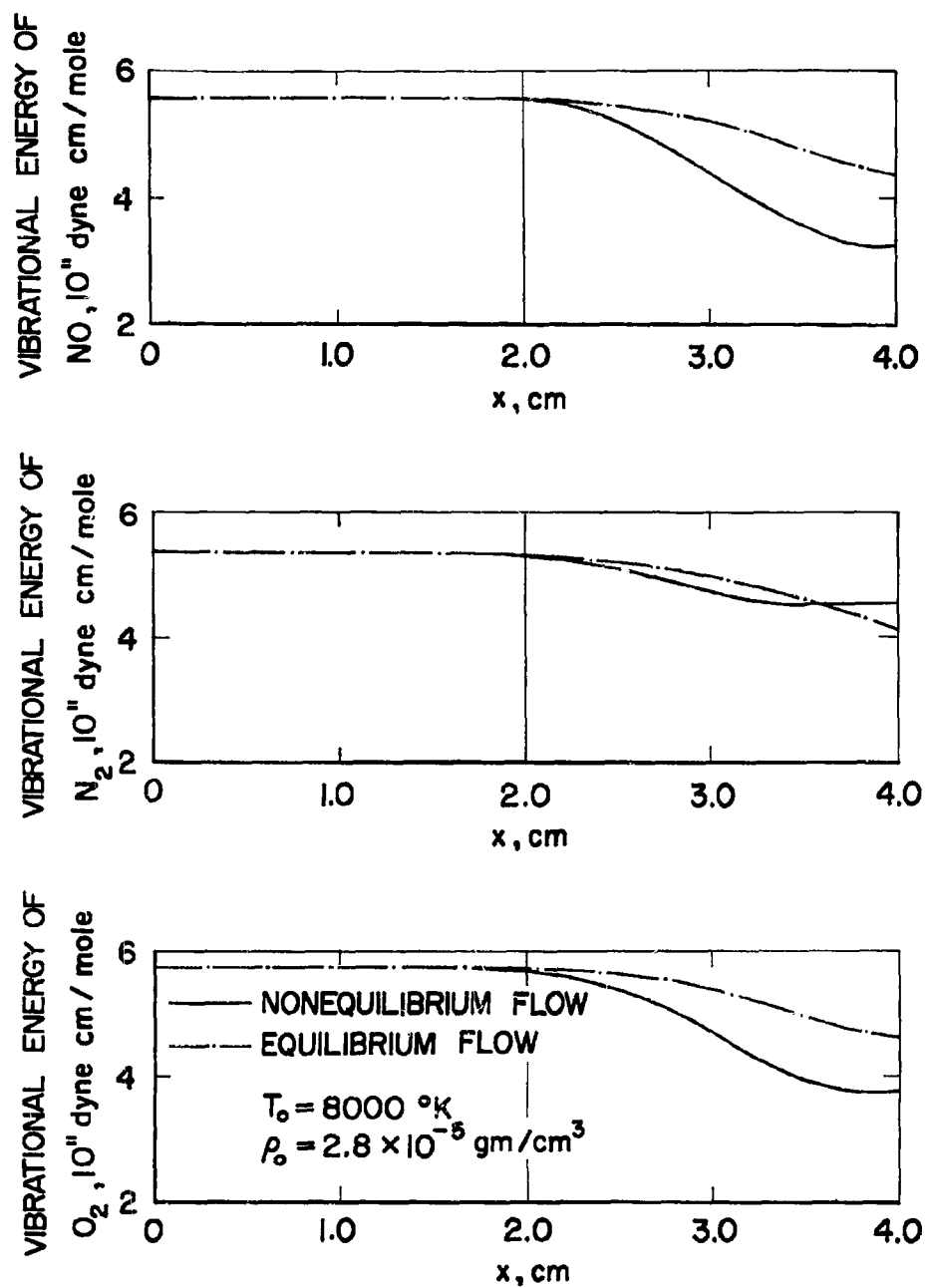
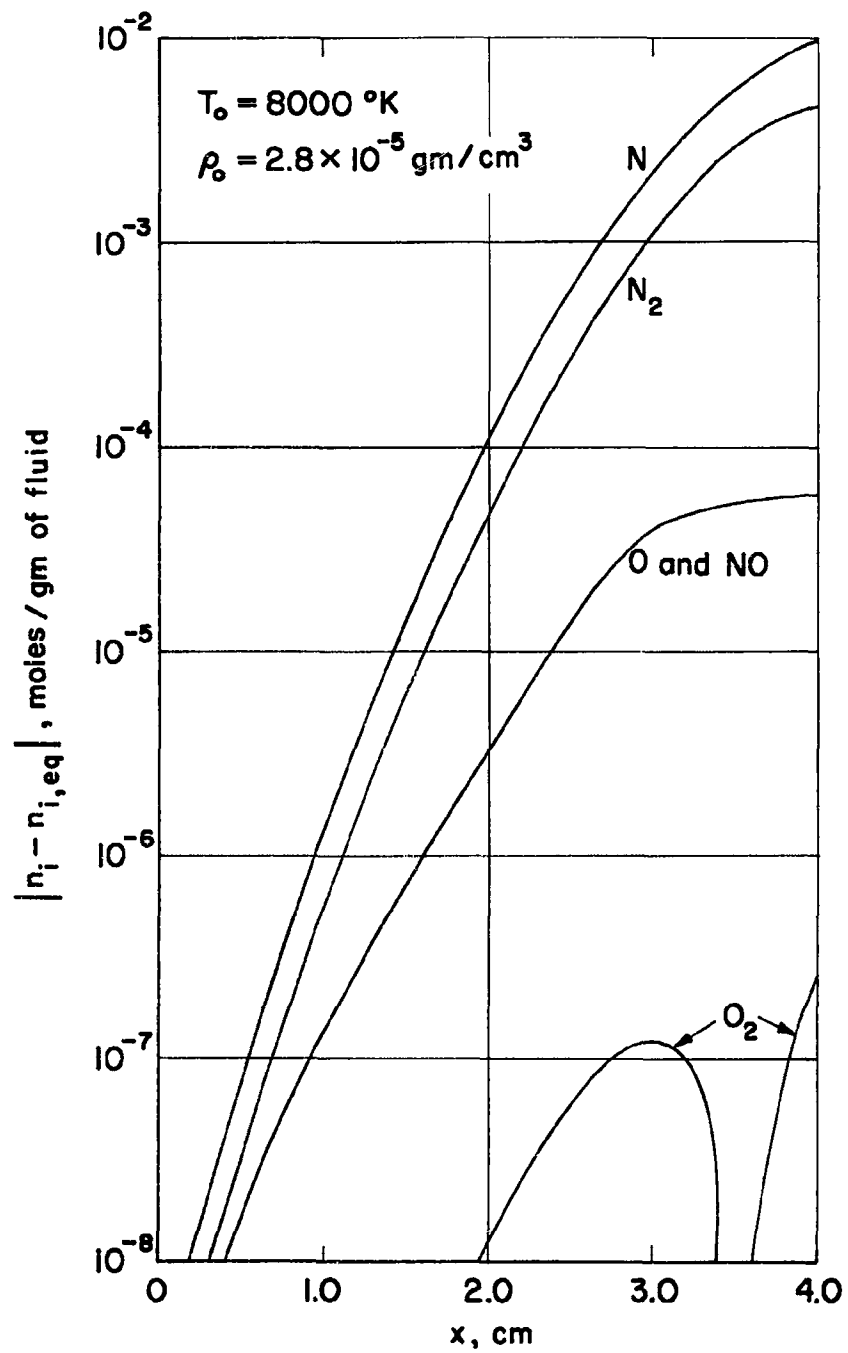


Fig. 10 Vibrational Energy

Fig. 11 $|n_i - n_{i,eq}|$

UNCLASSIFIED

UNCLASSIFIED
